



CHORUS

This is the accepted manuscript made available via CHORUS. The article has been published as:

Influence of nitrogen dopants on the magnetization of Co_3N clusters

Masahiro Sakurai, Xin Zhao, Cai-Zhuang Wang, Kai-Ming Ho, and James R. Chelikowsky
Phys. Rev. Materials **2**, 024401 — Published 6 February 2018

DOI: [10.1103/PhysRevMaterials.2.024401](https://doi.org/10.1103/PhysRevMaterials.2.024401)

Influence of nitrogen dopants on the magnetization of Co_3N clusters

Masahiro Sakurai,^{1,*} Xin Zhao,² Cai-Zhuang Wang,² Kai-Ming Ho,² and James R. Chelikowsky^{1,3,4}

¹*Center for Computational Materials, Institute for Computational Engineering and Sciences, The University of Texas at Austin, Austin, Texas 78712, USA*

²*Ames Laboratory, US DOE and Department of Physics and Astronomy, Iowa State University, Ames, Iowa 50011, USA*

³*Department of Chemical Engineering, The University of Texas at Austin, Austin, Texas 78712, USA*

⁴*Department of Physics, The University of Texas at Austin, Austin, Texas 78712, USA*

(Dated: January 12, 2018)

Using a real-space implementation of pseudopotentials within the density-functional theory, we show that the magnetization of a Co_3N cluster with a recently-discovered atomic structure is significantly affected by nitrogen dopants. In a Co_3N cluster with the hexagonal $P6_3/mmc$ structure, N dopants promote spin polarization for the Co- $3d$ electrons and the dopants themselves make additional contributions to net magnetic moment. These two factors enhance the total magnetic moment of a hexagonal Co_3N cluster, which can be as strong as bulk iron. In contrast, N dopants in a Co_3N cluster with the rhombohedral $R\bar{3}c$ structure degrade magnetic moment and the dopants are magnetically “inert,” which results in lower total magnetic moments in rhombohedral Co_3N clusters. These changes in magnetic moment originate from differences in the orbital hybridization between the Co- $3d$ and N- $2p$ states. We also examine how the magnetization of a Co_3N cluster depends on a N content. We find that the total magnetic moment of a hexagonal $\text{Co}_3\text{N}_{1+x}$ cluster with $-0.15 \leq x \leq 0.15$ is tunable and can be enhanced further by controlling the amount of nitrogen dopants.

I. INTRODUCTION

Owing to increasing demand in the global market for strong permanent magnets, accompanied by an insecure supply of rare-earth (RE) elements such as Nd, Sm and Dy, the theoretical design and experimental synthesis of new RE-free magnetic materials is a subject of an intensive study.¹ In the search of new magnetic materials without critical RE elements, three properties for high-performance magnets are desirable. These properties include a high saturation magnetization, a high magnetocrystalline anisotropy, and a high Curie temperature.

Among the various RE-free magnetic materials that have been explored, Fe- and Co-rich binary or ternary compounds are promising candidate materials. We expect the properties of such candidate materials might be improved by doping them with light elements. This is the case for popular RE-based permanent magnets such as $\text{Sm}_2\text{Fe}_{17}\text{N}_3$ and $\text{Nd}_2\text{Fe}_{12}\text{N}$ where theoretical and experimental work has shown that their magnetic properties can be improved by light elements such as N.^{2,3} In particular, doping with light elements for these RE compounds has resulted in stabilized atomic structures and improved magnetic properties.

Recent theoretical and experimental discoveries of Co-based new magnetic materials include Zr-Co and Hf-Co compounds,^{4,5} several metastable Co_nN ($n = 3, \dots, 8$) structures,⁶ Co_3Si and Co_3N in a nanoparticle form.^{7,8} Among these, Co_3N is an interesting system that have a potential to exhibit high magnetocrystalline anisotropy without losing large magnetization. In particular, the rhombohedral $R\bar{3}c$ structure (space group No. 167) is found to be the lowest-energy structure of Co_3N through crystal structure searches using an adaptive genetic algorithm (AGA)⁶ and has been successfully synthesized.⁸

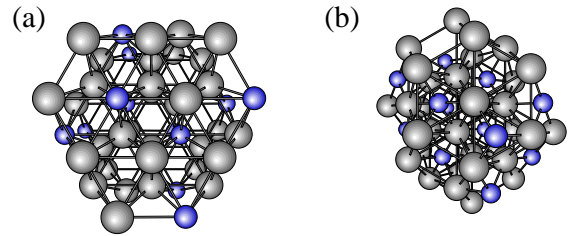


FIG. 1: Ball-and-stick model for $\text{Co}_{36}\text{N}_{12}$ clusters with (a) hexagonal $P6_3/mmc$ and (b) rhombohedral $R\bar{3}c$ structures. Gray and blue balls represent Co and N atoms, respectively.

In addition, Co_3N with the hexagonal $P6_3/mmc$ structure (space group No. 194), a new non-cubic structure of Co_3N , has been discovered recently in the form of nanoclusters and has also been identified as a metastable structure.⁸ Figure 1 shows the ball-and-stick model of a Co_3N cluster ($\text{Co}_{36}\text{N}_{12}$) with the hexagonal $P6_3/mmc$ and rhombohedral $R\bar{3}c$ structures. In spite of their potential magnetic properties, the role of nitrogen dopants on the magnetic properties has yet to be clarified.

Here, we employ a first-principles real-space pseudopotential method to investigate the effect of nitrogen dopants on the structural stability and magnetic properties of Co_3N clusters with recently-discovered hexagonal and rhombohedral structures. Structural stability of Co_3N clusters and its size dependence are analyzed by evaluating the formation energy. We investigate the total and local magnetic moments in elemental Co and doped Co_3N clusters to understand the role of nitrogen dopants on magnetization. We also examine the dependence of the total magnetic moment on a nitrogen content. We show that the magnetization of a hexagonal Co_3N cluster

can be enhanced further in a nitrogen-enriched condition, namely $\text{Co}_3\text{N}_{1+x}$ clusters with $x > 0$.

II. COMPUTATIONAL METHODS

We adopt a real-space formalism of pseudopotentials to obtain a self-consistent solution to the Kohn-Sham equation with in the density-functional theory (DFT).^{9,10} The formalism is implemented in the PARSEC code.^{11–13} The Laplacian in the kinetic-energy term is expanded by a high-order finite-differencing scheme with an orthogonal grid. We use a grid spacing of 0.3 a.u. (approximately 0.16 Å), which is fine enough to yield converged results for magnetic clusters containing 3d transition metals.^{14–16}

We obtain the Hartree potential by solving the Poisson equation using the conjugated gradient method.¹⁷ We calculate the exchange-correlation part using the generalized gradient approximation (GGA) functional.¹⁸ Interactions between the core and valence electrons are included using norm-conserving pseudopotentials, which were constructed from the Troullier-Martins recipe.¹⁹ Reference configurations for the pseudopotentials were taken to be $[\text{Ar}]4s^23d^74p^0$ for Co and $[\text{He}]2s^22p^3$ for N. The core radii were chosen to be $r_s = 2.18$, $r_d = 2.18$, and $r_p = 2.38$ a.u. for Co, and $r_s = 1.50$ and $r_p = 1.50$ a.u. for N (1 a.u. = 0.5292 Å). We included a partial core correction as well.²⁰

In the PARSEC code, wave functions and potentials are expressed on a Cartesian grid in *real space*, which is especially advantageous for non-periodic systems such as nanoclusters and two-dimensional materials. Instead of using a supercell approach, which is a standard technique in reciprocal-space electronic-structure calculations, we impose a finite domain boundary condition. Wave functions are sampled inside a spherical domain and vanish outside the domain boundary. The radius of a domain is set to be 10 a.u. larger than that of the cluster of interest, which ensures convergence of the total energy to less than ~ 1 meV/atom.

Owing to its nonlinear nature, the Kohn-Sham equation is solved by a self-consistent field (SCF) method, which involves a repetitive task of solving a linearized eigenvalue equation within an SCF loop. A solution at each SCF step is conventionally obtained by a diagonalization scheme. In PARSEC, the linearized Kohn-Sham equation is solved by a Chebyshev-filtered subspace iteration method.^{21,22} The code emphasizes the creation of a subspace rather than the computation of individual eigenvectors. The basis vectors are continually improved by filtering in the SCF cycle until converged. An improved filtering algorithm,²³ implemented in the most recent version of PARSEC, makes it possible to avoid a full diagonalization even at the initial SCF step. The filtering algorithm in PARSEC significantly reduces computational time to obtain a self-consistent solution in comparison to conventional diagonalization-based methods. The reduc-

TABLE I: Lattice constants and atomic positions of Co_3N in hexagonal $P6_3/mmc$ (space group No. 194) and rhombohedral $R\bar{3}c$ (space group No. 167) structures used in this work.

Lattice constants (Å)	Atomic (Wyckoff) positions		
Hexagonal $P6_3/mmc$			
$a = 5.03$, $c = 4.08$	Co	6h	(0.8315, 0.6630, 0.2500)
	N	2c	(0.3333, 0.6667, 0.2500)
Rhombohedral $R\bar{3}c$			
$a = 4.53$, $c = 13.05$	Co	18e	(0.6689, 0.0000, 0.2500)
	N	6b	(0.0000, 0.0000, 0.0000)

tion in computational time can be more than an order of magnitude.^{21,22}

III. RESULTS

A. Atomic structure

We list the lattice constants and atomic coordinates of Co_3N bulk in the hexagonal $P6_3/mmc$ and rhombohedral $R\bar{3}c$ crystal structures,^{6,8} which are used to generate atomic clusters of Co_3N , in Table I. The lattice constants of the $P6_3/mmc$ structure are taken from the experiment,⁸ while those of the $R\bar{3}c$ structure are from DFT calculations,⁶ which are very close to the experimental values.⁸ In the hexagonal $P6_3/mmc$ structure, the Co atom has eight neighboring Co atoms and four neighboring N atoms. In the rhombohedral $R\bar{3}c$ structure, the Co atom has fourteen neighbors including twelve Co atoms and two N atoms. The distances between neighboring Co atoms in rhombohedral Co_3N (2.60–2.63 Å) are slightly longer than those in hexagonal Co_3N (2.49–2.54 Å) as well as those in pristine hexagonal-close-packed (hcp) Co (2.50–2.51 Å). The nearest Co–N distance in rhombohedral Co_3N (1.87 Å) is much shorter than that in hexagonal Co_3N (2.50 Å).

Atomic clusters of Co_3N explored in this work are fragments of bulk Co_3N with the aforementioned crystal structures, as shown in Fig. 1. Clusters are taken to be spherical in shape. For selected sizes, a spherical Co_3N cluster is found to be more stable than other non-spherical ones because of a small surface-to-volume ratio and the absence of low coordinate surface atoms. **In order to clarify the role of nitrogen dopants on the structural stability and magnetic properties of Co_3N clusters, we also examine N-undoped Co clusters that are modeled by removing N atoms from Co_3N clusters with no relaxation allowed.**

Since we use bulk structures to generate atomic clusters, the interatomic forces in a generated cluster are small for interior atoms and are slightly larger for atoms near the surface of the cluster. We examined the effects of structural optimizations on the energetics and magnetic properties for clusters with selected sizes using

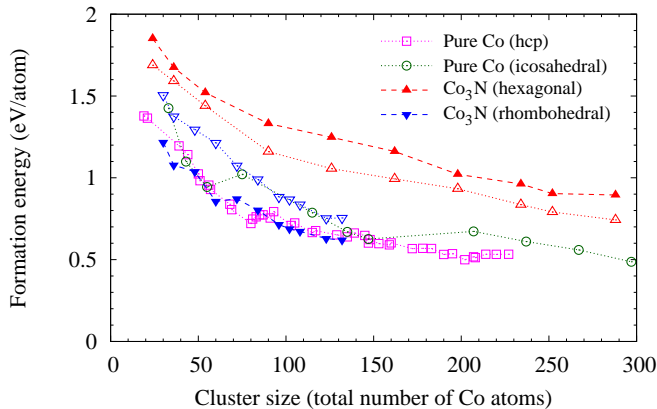


FIG. 2: The size dependence of the formation energies of hexagonal and rhombohedral Co_3N clusters (solid symbols) and N-undoped hexagonal and rhombohedral Co clusters (open symbols with the same colors). The formation energies of icosahedral and hcp Co clusters are also plotted for comparison.

the Broyden-Fletcher-Goldfarb-Shanno method^{24–26}. As a result, we find that changes due to structural optimization are less than 0.1 eV/atom for the formation energy. Corresponding changes in the magnetic moment are less than 0.1 μ_B per Co atom. The energetic and magnetic orderings that we will present in the following subsections are unlikely to be affected by structural optimization.

B. Formation energy

To investigate the structural stability of Co_3N clusters, we evaluated the formation energy per atom of a Co_3N cluster, which is defined as

$$E = \{E(\text{Co}_n\text{N}_m) - nE_{\text{Co}} - mE_{\text{N}}\}/(n + m). \quad (1)$$

Here, $E(\text{Co}_n\text{N}_m)$ is the total energy of a Co_3N cluster consisting of n Co atoms and m N atoms, E_{Co} is the total energy per atom of Co bulk in a hcp structure at the experimental lattice constants ($a = 2.51 \text{ \AA}$ and $c/a = 1.62$), and E_{N} is the total energy per atom for the N_2 molecule. A \vec{k} -point grid of $16 \times 16 \times 10$ was used to evaluate the total energy reference of hcp Co bulk. We note that Eq. (1) is applicable to N-undoped Co clusters ($m = 0$) as well as cobalt-nitride clusters with different compositions ($n/m \neq 3$).

Figure 2 illustrates the size dependence of the formation energies of Co_3N clusters in hexagonal and rhombohedral structures. For comparison, we plot the formation energies of N-undoped Co clusters in hexagonal and rhombohedral structures as well as pure Co clusters with icosahedral and hcp structures.¹⁵ In Fig. 2, clusters with lower formation energies are more stable than those with higher formation energies. We find that nitrogen dopants

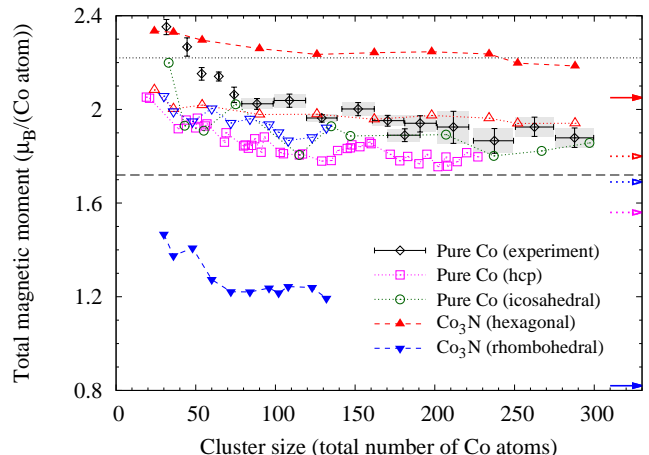


FIG. 3: The size dependence of the total magnetic moments of hexagonal and rhombohedral Co_3N clusters (solid symbols) and N-undoped hexagonal and rhombohedral Co clusters (open symbols with the same colors). The total magnetic moments of icosahedral and hcp Co clusters are also plotted for comparison. The arrows indicate the calculated total magnetic moments in bulk limit (see text for values). The dashed and dotted lines indicate the experimental total magnetic moments in hcp Co bulk ($1.72 \mu_B/\text{atom}$) and bcc Fe bulk ($2.22 \mu_B/\text{atom}$), respectively. We note that present calculations do not include the orbital moments, while experimental value is a full moment.

stabilize a Co cluster with a rhombohedral structure. Resulting rhombohedral Co_3N clusters are as stable as pure hcp Co clusters for sizes up to 140. Hexagonal Co clusters can accommodate nitrogen dopants at an energy cost of about 0.2 eV/atom for size ranges up to 300. As the cluster size increases, the formation energy becomes less dependent on a cluster size, approaching to a value in bulk limit.

C. Magnetic moment

Figure 3 shows the size dependence of total magnetic moments per Co atom of parent Co clusters and doped Co_3N ones in hexagonal and rhombohedral structures. In Fig. 3, we also plot the experimental values of pure Co clusters²⁷ for comparison. The arrows in Fig. 3 indicate the total magnetic moments in bulk limit that are evaluated by using a $10 \times 10 \times 12 \vec{k}$ -point grid for hexagonal Co_3N and a $8 \times 8 \times 3$ mesh for rhombohedral Co_3N . The total magnetic moments of N-undoped Co clusters in hexagonal and rhombohedral structures are comparable to or slightly larger than those of pure Co clusters with icosahedral and hcp structures. This trend is expected to continue towards bulk limit where hexagonal and rhombohedral Co phases are predicted to have the total magnetic moments of 1.80 and 1.69 μ_B/atom , respectively. Owing to the omission of orbital contributions

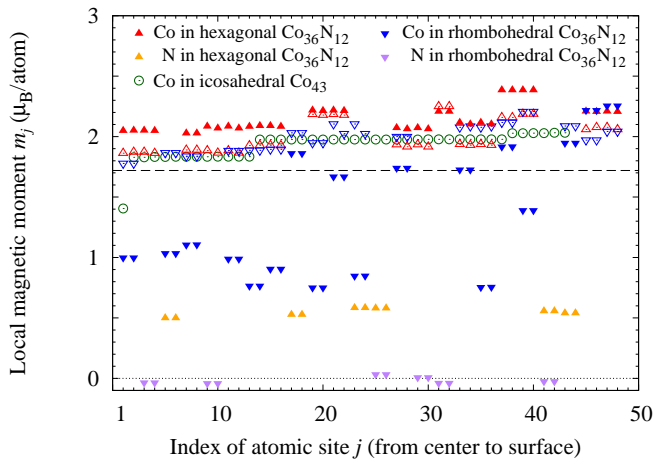


FIG. 4: Evolution of local magnetic moments in hexagonal and rhombohedral $\text{Co}_{36}\text{N}_{12}$ clusters (solid symbols). The local magnetic moments of parent (N-undoped) Co_{36} clusters (open symbols in red and blue) and icosahedral Co_{43} cluster (open green circles) are plotted for comparison. The dashed line indicates the experimental full magnetic moment of hcp Co bulk ($1.72 \mu_B/\text{atom}$).

to the moments, the total magnetic moment obtained for hcp Co bulk ($1.56 \mu_B/\text{atom}$) is slightly smaller than the experimental value of $1.72 \mu_B/\text{atom}$.

With nitrogen doping, the total magnetic moment is significantly increased in hexagonal Co_3N clusters. The calculated magnetic moments are well above those of pristine Co clusters and are comparable to the experimental full moment of bulk iron ($2.22 \mu_B$ per Fe atom including the orbital contributions). The increase in the magnetic moment is about $0.3 \mu_B$ per Co atom over a wide range of cluster sizes. In bulk limit, hexagonal Co_3N is predicted to have the total magnetic moment of $2.05 \mu_B$ per Co atom. In contrast, there is a considerable decrease in the magnetic moment of rhombohedral Co_3N clusters. In its bulk limit, rhombohedral Co_3N is predicted to have the total magnetic moment of $0.82 \mu_B$ per Co atom, which is nearly a half of that of hcp Co bulk and is narrowly larger than that of bulk nickel ($0.61 \mu_B$ per Ni atom including the orbital contributions).

In order to analyze the change in the total magnetic moment from nitrogen doping, we decompose the total magnetic moment into local magnetic moments, which are defined as

$$m_j = \int_{\Omega_j} [\rho_{\uparrow}(\vec{r}) - \rho_{\downarrow}(\vec{r})] d^3r. \quad (2)$$

Here, $\rho_{\uparrow(\downarrow)}$ represents the electron density of the majority (minority) spin and Ω_j denotes a spherical domain centered on an atom with a label j (site index). The radius of the sphere is chosen to be half of the shortest inter-atomic bond. We confirm that the sum of the local magnetic moments ($\sum_j m_j$) is nearly equal to the total

magnetic moment and is not sensitive to the choice of our radius.

Figure 4 shows atomic-site-resolved magnetic moments for hexagonal and rhombohedral $\text{Co}_{36}\text{N}_{12}$ clusters as well as those of N-undoped Co clusters. Without nitrogen dopants, both hexagonal and rhombohedral Co_{36} clusters have bulk-like local magnetic moments in a cluster interior and the moments gradually increase when going from the center to a surface. This trend is consistent with the local magnetic moments of a similar-sized icosahedral Co_{43} cluster and has been observed before in Fe clusters.¹⁴ In a hexagonal $\text{Co}_{36}\text{N}_{12}$ cluster, it is evident that local magnetic moments are enhanced at the Co sites. Nitrogen dopants lead to $m_j > 2.0 \mu_B$ for all Co sites. Moreover, nitrogen dopants themselves become magnetic ($m_j \sim 0.5 \mu_B$), making additional contributions to net magnetic moment. These two factors cooperatively bring about a large increase in the total magnetic moment of hexagonal Co_3N clusters. In a rhombohedral $\text{Co}_{36}\text{N}_{12}$ cluster, local magnetic moments are substantially suppressed at most of the Co sites. In particular, significant decrease is observed in the inner Co sites. Nitrogen sites are magnetically “inert,” making no contribution to net magnetic moment. These two unfavorable factors account for the reduced total magnetic moment in rhombohedral Co_3N clusters.

D. Density of states

Nitrogen dopants in a Co_3N cluster cause an opposite effect on the total and local magnetic moments depending on the atomic structure of a cluster. In order to understand this behavior, we analyze the electronic density of states (DOS). Figure 5 shows the total and partial DOS for hexagonal and rhombohedral $\text{Co}_{36}\text{N}_{12}$ clusters. The total DOS of a parent Co_{36} cluster is also shown for comparison. As expected, overall shape of total DOS comes from the Co- $3d$ states for both cases. In a hexagonal $\text{Co}_{36}\text{N}_{12}$ cluster, the N- $2p$ states span a wide range of energies. As a result of an increase in electronic states arising from the N- $2p$ electrons, we observe new “shoulder” features in total DOS for majority spin at around -4 and -0.8 eV. An increase in the total DOS for minority spins is also found below -2 eV, although the increase is smaller than that of majority spin. In a rhombohedral $\text{Co}_{36}\text{N}_{12}$ cluster, the spectrum of total DOS for majority spin is shifted to higher energy, accompanied by a reduced peak height. For both majority-spin and minority-spin channels, the N- $2p$ states are found below -3.5 eV where the $2p$ states hybridize with the Co- $3d$ states. These hybridized orbitals form low-energy bonding states that are magnetically “inert.” The analyses on DOS performed here clearly show that sizable changes in the total and local magnetic moments of Co_3N clusters originate from the difference in an orbital hybridization between the Co- $3d$ and N- $2p$ states.

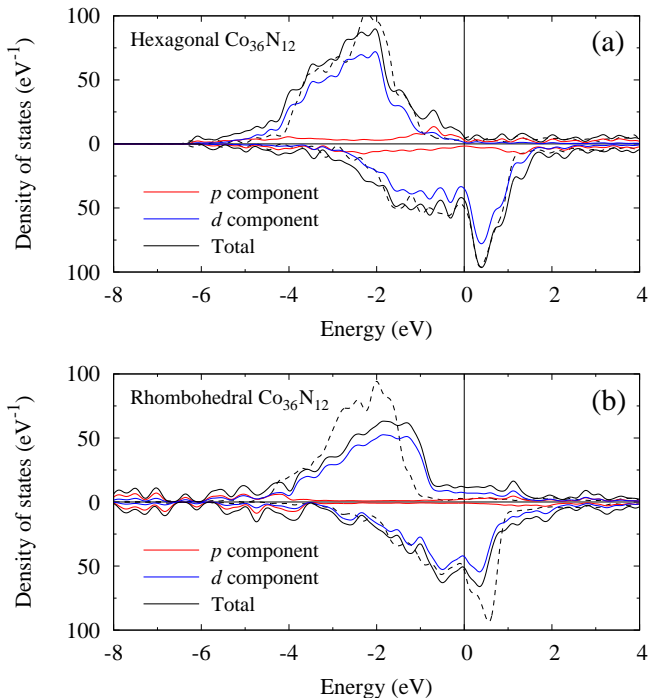


FIG. 5: Total density of states (DOS) and partial DOS for p and d orbitals in (a) hexagonal $\text{Co}_{36}\text{N}_{12}$ and (b) rhombohedral $\text{Co}_{36}\text{N}_{12}$ clusters for majority spin (upper panel) and minority spin (lower panel). The dashed line indicates the total DOS of a parent (N-undoped) Co_{36} cluster. A Gaussian broadening of 0.1 eV is used. Energy is measured from the Fermi energy.

E. Composition dependence

Owing to the presence of a surface, atomic clusters synthesized in experiment may not correspond to a Co_3N composition. Here, we examine the influence of composition change on the structural stability and total magnetic moment. We focus on hexagonal $\text{Co}_3\text{N}_{1+x}$ clusters with $-0.15 \leq x \leq 0.15$ and with sizes of containing up to 200 Co atoms (up to approximately 1.8 nm in diameter).

Figure 6(a) shows the formation energies, evaluated by using Eq. (1), for various hexagonal $\text{Co}_3\text{N}_{1+x}$ clusters with different compositions. Most of the formation energies of $\text{Co}_3\text{N}_{1+x}$ clusters with $x \neq 0$ are on and around the “interpolated” lines that connect the values of perfect Co_3N clusters. The examined $\text{Co}_3\text{N}_{1+x}$ clusters are nearly as stable as perfect Co_3N ones, indicating that $\text{Co}_3\text{N}_{1+x}$ clusters are viable candidate structures.

In Fig. 6(b), the total magnetic moments of various hexagonal $\text{Co}_3\text{N}_{1+x}$ clusters are compared to those of perfect Co_3N clusters. In the size range we explored, most of the calculated magnetic moments of hexagonal $\text{Co}_3\text{N}_{1+x}$ clusters are found to be comparable to the experimental full moment of bulk iron ($2.22 \mu_B$ per Fe atom including the orbital contributions). In comparison to a weak size dependence of the total magnetic moments of

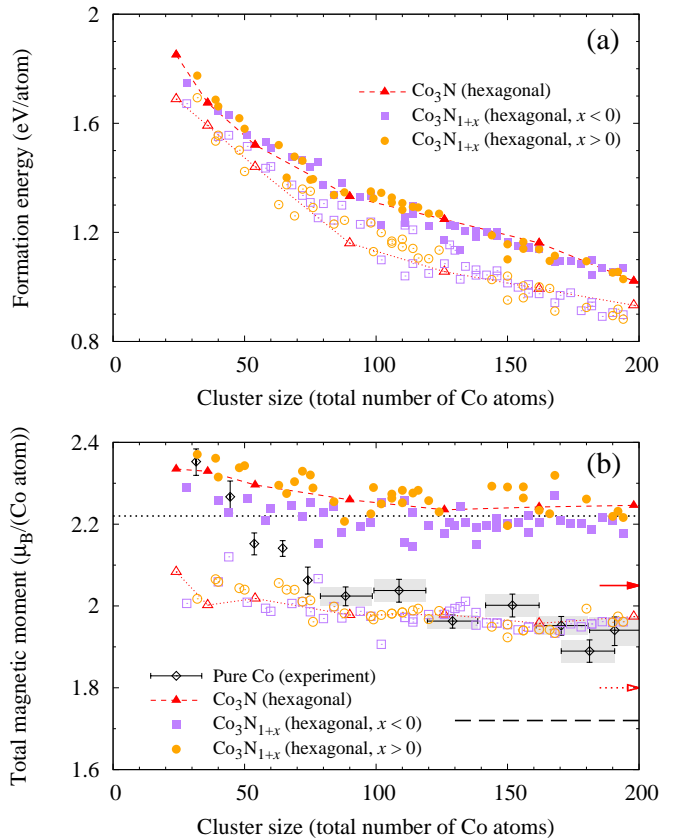


FIG. 6: The size dependences of (a) formation energies and (b) total magnetic moment for hexagonal $\text{Co}_3\text{N}_{1+x}$ clusters with $-0.15 \leq x \leq 0.15$ (solid symbols). The formation energies and total magnetic moments of parent (N-undoped) Co clusters are also plotted using open symbols with the same colors. The red arrows in (b) indicate calculated total magnetic moments in bulk limit (see text for values). The dashed and dotted lines in (b) indicate the experimental total magnetic moments in hcp Co bulk ($1.72 \mu_B/\text{atom}$) and bcc Fe bulk ($2.22 \mu_B/\text{atom}$), respectively. We note that present calculations do not include orbital moments, while experimental value is a full moment.

parent Co clusters, the total magnetic moments obtained for $\text{Co}_3\text{N}_{1+x}$ clusters are largely scattered, indicating a strong dependence of the magnetic moment on a nitrogen content. The total magnetic moments of $\text{Co}_3\text{N}_{1+x}$ clusters with $x < 0$ (namely, nitrogen-“deficient” clusters) tend to be lower than those of perfect Co_3N clusters, while $\text{Co}_3\text{N}_{1+x}$ clusters with $x > 0$ (namely, nitrogen-“enriched” clusters) tend to have a larger magnetic moment.

The aforementioned trend is evident in Fig. 7 where total magnetic moments are plotted as a function of x for hexagonal $\text{Co}_3\text{N}_{1+x}$ clusters containing 50–100 Co atoms with different compositions. There is a gradual increase in magnetic moment from a nitrogen-“deficient” regime ($x < 0$) to a nitrogen-“enriched” regime ($x > 0$). The to-

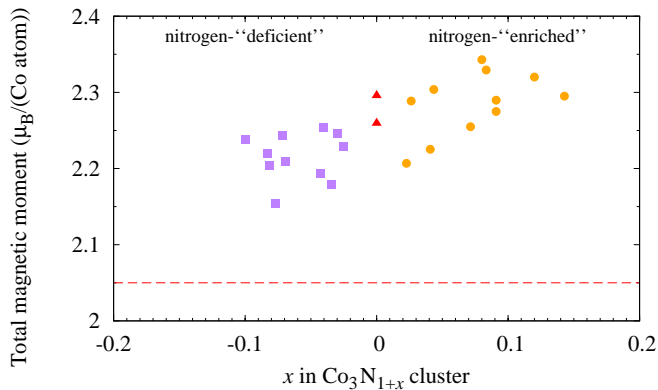


FIG. 7: Total magnetic moments of hexagonal $\text{Co}_3\text{N}_{1+x}$ clusters that contain 50–100 Co atoms with different nitrogen contents. The red dashed line indicates the magnetic moment of hexagonal Co_3N bulk ($2.05 \mu_B/\text{atom}$, present calculation neglecting the orbital moments).

tal magnetic moment may be maximized with an optimal composition of $x \sim 0.1$. We suggest that the magnetization of a hexagonal Co_3N cluster, which is as large as that of bulk iron, is tunable and can be increased further by controlling the amount of nitrogen dopants.

IV. SUMMARY

We examined the structural stability and magnetic properties of Co_3N clusters using real-space pseudopotentials constructed within the density-functional theory.

We show that nitrogen dopants can have a notable influence on the magnetization of Co_3N clusters depending on the atomic structure of a cluster. In particular, Co_3N clusters with the hexagonal $P6_3/mmc$ structure are predicted to have a large total magnetic moment, which can be as strong as bulk iron. On the other hand, Co_3N clusters with the rhombohedral $R\bar{3}c$ structure have a significantly suppressed total magnetic moment. We have clarified that the changes in the total and local magnetic moments due to nitrogen doping originate from the difference in an orbital hybridization between the Co- $3d$ and N- $2p$ states. We have also examined the dependence of the total magnetic moment on a nitrogen content. We suggest that the total magnetic moment of a hexagonal $\text{Co}_3\text{N}_{1+x}$ cluster can be maximized by tuning the amount of nitrogen dopants.

Acknowledgments

We thank Dr. Balamurugan Balasubramanian (University of Nebraska, Lincoln) for providing us with the crystal structure of Co_3N bulk in the hexagonal $P6_3/mmc$ structure in prior to publication. M.S. and J.R.C. acknowledge support from a grant from the National Science Foundation (NSF), DMREF-1729202. X.Z., C.-Z.W. and K.-M.H. acknowledge support from a grant from the NSF, DMREF-1729677. HPC resources were provided by the Texas Advanced Computing Center (TACC) at The University of Texas at Austin as part of the Extreme Science and Engineering Discovery Environment (XSEDE), which is supported by the NSF grant No. ACI-1548562, through XSEDE allocation MCA08X029.

* Electronic address: masahiro@ices.utexas.edu

¹ J. M. D. Coey, *Scripta Mater.* **67**, 524 (2012).

² J. M. D. Coey and H. Sun, *J. Magn. Magn. Mater.* **87**, L251 (1990).

³ T. Miyake, K. Terakura, Y. Harashima, H. Kino, and S. Ishibashi, *J. Phys. Soc. Jpn.* **83**, 043702 (2014).

⁴ X. Zhao, M. C. Nguyen, W. Y. Zhang, C. Z. Wang, M. J. Kramer, D. J. Sellmyer, X. Z. Li, F. Zhang, L. Q. Ke, V. P. Antropov, and K. M. Ho, *Phys. Rev. Lett.* **112**, 045502 (2014).

⁵ B. Balamurugan, B. Das, W. Y. Zhang, R. Skomski, and D. J. Sellmyer, *J. Phys.: Condens. Matter* **26**, 064204 (2014).

⁶ X. Zhao, L. Ke, C.-Z. Wang, and K.-M. Ho, *Phys. Chem. Chem. Phys.* **18**, 31680 (2016).

⁷ B. Balasubramanian, P. Manchanda, R. Skomski, P. Mukherjee, S. R. Valloppilly, B. Das, G. C. Hadjipanayis, and D. J. Sellmyer, *Appl. Phys. Lett.* **108**, 152406 (2016).

⁸ B. Balasubramanian, X. Zhao, S. R. Valloppilly, S. Benawal, R. Skomski, A. Sarella, X. Li, X. Xu, H. Cao, H. Wang, A. Enders, C.-Z. Wang, K.-M. Ho, and D. J.

Sellmyer, (*under review in Nano Lett.*).

⁹ P. Hohenberg and W. Kohn, *Phys. Rev.* **136**, B864 (1964).

¹⁰ W. Kohn and L. J. Sham, *Phys. Rev.* **140**, A1133 (1965).

¹¹ J. R. Chelikowsky, N. Troullier, and Y. Saad, *Phys. Rev. Lett.* **72**, 1240 (1994).

¹² J. R. Chelikowsky, N. Troullier, K. Wu, and Y. Saad, *Phys. Rev. B* **50**, 11355 (1994).

¹³ L. Kronik, A. Makmal, M. L. Tiago, M. M. G. Alemany, M. Jain, X. Huang, Y. Saad, and J. R. Chelikowsky, *Phys. Status Solidi B* **243**, 1063 (2006).

¹⁴ M. L. Tiago, Y. Zhou, M. M. G. Alemany, Y. Saad, and J. R. Chelikowsky, *Phys. Rev. Lett.* **97**, 147201 (2006).

¹⁵ J. Souto-Casares, M. Sakurai, and J. R. Chelikowsky, *Phys. Rev. B* **93**, 174418 (2016).

¹⁶ M. Sakurai, J. Souto-Casares, and J. R. Chelikowsky, *Phys. Rev. B* **94**, 024437 (2016).

¹⁷ Y. Saad, *Iterative Methods for Sparse Linear Systems*, 2nd ed. (Society for Industrial and Applied Mathematics, 2003).

¹⁸ J. P. Perdew, K. Burke, and M. Ernzerhof, *Phys. Rev. Lett.* **77**, 3865 (1996).

¹⁹ N. Troullier and J. L. Martins, *Phys. Rev. B* **43**, 1993

- (1991).
- ²⁰ S. G. Louie, S. Froyen, and M. L. Cohen, *Phys. Rev. B* **26**, 1738 (1982).
- ²¹ Y. Zhou, Y. Saad, M. L. Tiago, and J. R. Chelikowsky, *Phys. Rev. E* **74**, 066704 (2006).
- ²² Y. Zhou, Y. Saad, M. L. Tiago, and J. R. Chelikowsky, *J. Comput. Phys.* **219**, 172 (2006).
- ²³ Y. Zhou, J. R. Chelikowsky, and Y. Saad, *J. Comput. Phys.* **274**, 770 (2014).
- ²⁴ R. H. Byrd, P. Lu, J. Nocedal, and C. Zhu, *SIAM J. Sci. Comput.* **16**, 1190 (1995).
- ²⁵ C. Zhu, R. H. Byrd, P. Lu, and J. Nocedal, *ACM Trans. Math. Software* **23**, 550 (1997).
- ²⁶ J. L. Morales and J. Nocedal, *ACM Trans. Math. Software* **38**, 1 (2011).
- ²⁷ I. M. Billas, A. Châtelain, and W. A. de Heer, *Science* **265**, 1682 (1994).